Title
The Discovery of a Gravitationally Lensed Supernova Ia at Redshift 2.22

Journal
The Astrophysical Journal, 866(1)

ISSN
0004-637X

Authors
Rubin, D
Hayden, B
Huang, X
et al.

Publication Date
2018-10-10

DOI
10.3847/1538-4357/aad565

Peer reviewed

DRAFT VERSION JULY 18, 2017
Typeset using LaTeX default style in AASTeX61

THE DISCOVERY OF A GRAVITATIONALLY LENSED SUPERNOVA IA AT REDSHIFT 2.22

D. RUBIN,[1,2] B. HAYDEN,[2,3] X. HUANG,[4] G. ALDERING,[2] R. AMANULLAH,[5] K. BARBARY,[2] K. BOONE,[2,3] M. BRODWIN,[6] S. E. DEUSTUA,[1] S. DIXON,[2,3] P. EISENHARDT,[7] A. S. FRUCHTER,[1] A. H. GONZALEZ,[8] A. GOOBAR,[5] R. R. GUPTA,[2] I. HOOK,[9] M. J. JEE,[10] A. G. KIM,[2] M. KOWALSKI,[11] C. E. LIDMAN,[12] E. LINDER,[2] K. LUTHER,[2,3] J. NORDIN,[11] R. PAIN,[13] S. PERLMUTTER,[2,3] Z. RAHA,[4,2] M. RIGAULT,[11] P. RUIZ-LAPUENTE,[14,15] C. M. SAUNDERS,[2,3,13] C. SOFIATTI,[2,3] A. L. SPADAFORA,[2] S. A. STANFORD,[16] D. STERN,[7] N. SUZUKI,[17] AND S. C. WILLIAMS[9]
(THE SUPERNOVA COSMOLOGY PROJECT)

[1]*Space Telescope Science Institute, 3700 San Martin Drive, Baltimore, MD 21218*
[2]*E.O. Lawrence Berkeley National Lab, 1 Cyclotron Rd., Berkeley, CA, 94720*
[3]*Department of Physics, University of California Berkeley, Berkeley, CA 94720*
[4]*Department of Physics and Astronomy, University of San Francisco, San Francisco, CA 94117-1080*
[5]*The Oskar Klein Centre, Department of Physics, AlbaNova, Stockholm University, SE-106 91 Stockholm, Sweden*
[6]*Department of Physics and Astronomy, University of Missouri-Kansas City, Kansas City, MO 64110*
[7]*Jet Propulsion Laboratory, California Institute of Technology, Pasadena, CA, 91109*
[8]*Department of Astronomy, University of Florida, Gainesville, FL 32611*
[9]*Physics Department, Lancaster University, Lancaster LA1 4YB, United Kingdom*
[10]*Department of Astronomy and Center for Galaxy Evolution Research, Yonsei University, 50 Yonsei-ro, Seoul 03772, Korea*
[11]*Institut für Physik, Newtonstr. 15, 12489 Berlin, Humboldt-Universität zu Berlin, Germany*
[12]*Australian Astronomical Observatory, PO Box 296, Epping, NSW 1710, Australia*
[13]*Laboratoire de Physique Nucleaire et de Hautes Energies, Universite Pierre et Marie Curie, 75252 Paris Cedec 05, France*
[14]*Institute of Cosmos Sciences, University of Barcelona, E-08028 Barcelona, Spain*
[15]*Instituto de Fisica Fundamental, CSIC, E-28006 Madrid, Spain*
[16]*Department of Physics, University of California Davis, One Shields Avenue, Davis, CA 95616*
[17]*Kavli Institute for the Physics and Mathematics of the Universe, University of Tokyo, Kashiwa, 277-8583, Japan*

Submitted to ApJ

ABSTRACT

We present the discovery and measurements of a gravitationally lensed supernova (SN) behind the galaxy cluster MOO J1014+0038. Based on multi-band *Hubble Space Telescope* and Very Large Telescope (VLT) photometry and spectroscopy, we find a 99% probability that this SN is a SN Ia, and a 1% chance of a CC SN. Our typing algorithm combines the shape and color of the light curve with the expected rates of each SN type in the host galaxy. With a redshift of 2.2216, this is the highest redshift SN Ia discovered with a spectroscopic host-galaxy redshift. A further distinguishing feature is that the lensing cluster, at redshift 1.23, is the most distant to date to have an amplified SN. The SN lies in the middle of the color and light-curve shape distributions found at lower redshift, disfavoring strong evolution to $z = 2.22$. We estimate an amplification of $2.8^{+0.6}_{-0.5}$ (1.10 ± 0.23 mag)—compatible with the value estimated from the weak-lensing-derived mass and the mass-concentration relation from ΛCDM simulations—making it the most amplified SN Ia discovered behind a galaxy cluster.

Keywords: cosmology: observations — gravitational lensing — galaxies: clusters: individual (MOO J1014+0038) supernovae: general

Corresponding author: David Rubin
drubin@stsci.edu

1. INTRODUCTION

Gravitational lensing by massive galaxy clusters offers an amplified and magnified view of the high-redshift universe. Several examples of supernovae (SNe) lensed by foreground clusters have been found in recent years (Goobar et al. 2009; Amanullah et al. 2011; Nordin et al. 2014; Patel et al. 2014; Kelly et al. 2015; Rodney et al. 2015a; Petrushevska et al. 2016). Four of these cluster-lensed SNe have been of Type Ia (SNe Ia), from which the amplification due to lensing has been determined. (Two additional SNe Ia that were lensed by field galaxies have also been found, Quimby et al. 2014; Goobar et al. 2017; we summarize all referenced SNe in Table 1).

The uniquely precise standardization possible with SNe Ia provides amplification information, breaking the so-called mass-sheet degeneracy that is problematic for most shear-based lensing models, and permits independent direct tests of cluster mass models obtained from galaxy lensing (Nordin et al. 2014; Patel et al. 2014; Rodney et al. 2015a). Lenses that produce multiple SN images provide additional model constraints (Kelly et al. 2016a). To date the redshifts of gravitationally lensed background SNe Ia have been at $z < 1.39$, a redshift range where even without lensing the complete (normal) SN Ia population can be detected using single-orbit *HST* visits. In cases of stronger amplification of sources beyond the redshift reach of normal observations, tests of SN Ia properties and rates over a larger look-back time become possible. Here we report the discovery of the most amplified SN Ia behind a galaxy cluster ever found, with a spectroscopic host-galaxy redshift making it also the most distant.

2. DISCOVERY

The Supernova Cosmology Project "See Change" program (PI: Perlmutter, PIDs: 13677 and 14327) monitored twelve massive galaxy clusters in the redshift range 1.13 to 1.75 with *Hubble Space Telescope* (*HST*) Wide Field Camera 3 (WFC3), with the goals of greatly expanding the range of the high-redshift Hubble diagram and accurately determining high-redshift cluster masses via weak lensing. We observed each cluster with one orbit (split between $F814W$, $F105W$, and $F140W$) at a roughly 5-week observer-frame cadence. The supernova survey was very deep; our 50% completeness for simulated SN detection was AB 26.5 in $F105W + F140W$ (Hayden et al. in prep.); this is ~ 1 magnitude fainter than a $z = 1.75$ SN Ia at maximum.[1] When a promising Type Ia supernova candidate was found, at least one extra visit was triggered and executed within 2–3 observer frame weeks after the initial discovery. These visits provided better light-curve sampling, usually close to maximum light, and frequently extended the wavelength range with $F160W$.

On 2016 Feb 29 UTC, we searched images of the WISE-selected (Wright et al. 2010) massive galaxy cluster MOO J1014+0038 ($z = 1.23$, Decker et al. in prep.; $M_{200} = (5.6 \pm 0.6) \times 10^{14} M_\odot$, Brodwin et al. 2015), from the Massive and Distant Clusters of WISE Survey (MaDCoWS; Gettings et al. 2012, Stanford et al. 2014, Gonzalez et al. 2015). We detected a red (WFC3 $F140W = 25.1$, $F105W - F140W = 1.4$ AB mag; upper limit only in $F814W$) supernova at $\alpha = 153.^\circ52655$, $\delta = +0.^\circ64041$ (J2000, aligned to USNO-B1). This SN was internally designated as SN SCP16C03,[2] as it was the third SN found in this cluster field (alphabetically labeled cluster "C") in 2016. As shown in Figure 1, the SN lies on a red galaxy having a color of $F105W - F140W = 1.5$ AB mag and is located $0.''7$ from the core of this galaxy ($\alpha = 153.^\circ52643$, $\delta = +0.^\circ64025$). We conclude that this galaxy must be the host galaxy; there are no other galaxies nearby, and the light curve is incompatible with those possible from an intra-cluster SN within MOO J1014+0038 (as discussed in Section 6).

3. PHOTOMETRIC AND SPECTROSCOPIC FOLLOWUP

We activated ToO spectroscopic observations (PI: Hook) using X-shooter, the multi-wavelength medium resolution spectrograph on the Very Large Telescope (Vernet et al. 2011). Five "Observation Blocks" were taken between 2016 Mar 4-5 (UT), yielding a total integration time of 3.8, 4.4, and 5.0 hours in the X-shooter UVB, VIS, and NIR arms, respectively. Although the slit orientation captured both the host galaxy and the SN, the galaxy was ~ 4 magnitudes brighter, so we only were able to extract a host-galaxy spectrum. The data were reduced to wavelength- and flux-calibrated, sky-subtracted, 2D spectra using the Reflex software (Freudling et al. 2013). Optimal 1D-extractions were determined using a combination of custom and `IRAF` routines.[3] These extractions were combined (with a weighted mean) to create a final 1D spectrum. We corrected for telluric absorption using a model atmosphere computed by the Line-By-Line Radiative Transfer Model (Clough et al. 1992; Clough et al. 2005) retrieved through Telfit (Gullikson et al. 2014). The host-galaxy spectrum is shown in Figure 2. Several absorption lines are clearly detected, resulting in a weighted cross correlation redshift of 2.2216 ± 0.0002 for the host galaxy. No emission lines were detected.

[1] When stacking all the epochs together, we reach 5σ point-source depths of AB 28.0 in $F105W$ and AB 27.9 in $F140W$.

[2] Nicknamed "Joseph."

[3] IRAF is distributed by the National Optical Astronomy Observatories, which are operated by the Association of Universities for Research in Astronomy, Inc., under cooperative agreement with the National Science Foundation.

Table 1. Other high-redshift or gravitationally lensed SNe.

SN	Redshift	Redshift Type	Lens	Lens Redshift	Amplification	Type	Reference
CAND-ISAAC	0.64	Spec	Cluster	0.18	3.6	IIP	Goobar et al. (2009); Stanishev et al. (2009)
PS1-10afx	1.39	Spec	Field	1.12	30[a]	Ia	Quimby et al. (2014)
A1, CLA11Tib	1.14	Spec	Cluster	0.19	1.4	Ia	Nordin et al. (2014); Patel et al. (2014)
H1, CLN12Did	0.85	Spec	Cluster	0.35	1.3	Ia	Nordin et al. (2014); Patel et al. (2014)
L2, CLO12Car	1.28	Spec	Cluster	0.39	1.7	Ia	Nordin et al. (2014); Patel et al. (2014)
Refsdal	1.49	Spec	Cluster	0.54	~ 100[a]	II	Kelly et al. (2015, 2016b)
HFF14Tom	1.35	Spec	Cluster	0.31	1.7	Ia	Rodney et al. (2015a)
GND13Sto	1.80 ± 0.02	Phot	···	···	···	Ia	Rodney et al. (2015b)
GND12Col	$2.26^{+0.02}_{-0.10}$	Phot	···	···	···	Ia	Rodney et al. (2015b)
CAND-669	0.67	Spec	Cluster	0.18	1.3	IIL	Petrushevska et al. (2016)
CAND-821	1.70	Spec	Cluster	0.18	4.3	IIn	Amanullah et al. (2011); Petrushevska et al. (2016)
CAND-1392	0.94	Spec	Cluster	0.18	2.7	IIP	Petrushevska et al. (2016)
CAND-10658	$0.94^{+0.07}_{-0.27}$	Spec	Cluster	0.18	1.7	IIn	Petrushevska et al. (2016)
CAND-10662	$1.03^{+0.20}_{-0.17}$	Spec	Cluster	0.18	2.6	IIP	Petrushevska et al. (2016)
iPTF16geu	0.41	Spec	Field	0.22	52[a]	Ia	Goobar et al. (2017)
SCP16C03 (“Joseph”)	2.22	Spec	Cluster	1.23	2.8	Ia	This Work

[a] Multiple images; amplification is sum over all images.

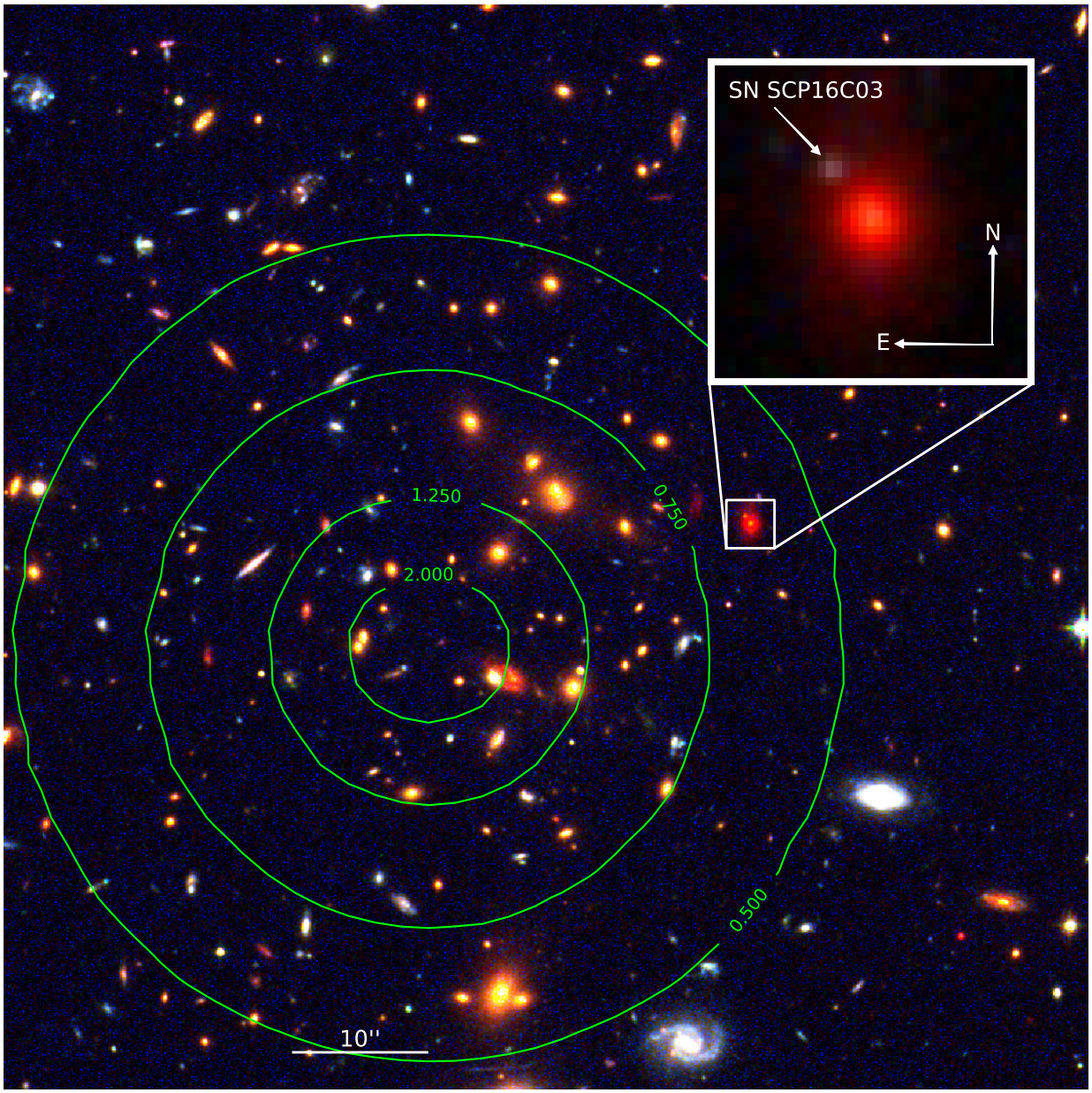

Figure 1. Color image of the central part of MOO J1014+0038 made with an $F814W$ stack and the $F105W$ and $F160W$ from our first triggered *HST* imaging near maximum light. The inset panel uses different scaling, and only IR data ($F105W$, $F125W$, and $F160W$). The compass arrows are $1''$ in linear scale. Both panels use hyperbolic arcsine intensity scaling. In green, we show contours of our computed lensing amplification model (in magnitudes), described in Section 8.

This SN was $15''$ away from the center of a dense concentration of cluster galaxies. Assuming the optical center is the halo center and an NFW mass profile (Navarro et al. 1997), we initially estimated an amplification of ~ 2.2 in flux. Based on the likelihood that we were observing a highly magnified, high-redshift SN Ia, we were granted Director's Discretionary *HST* time for this unique object, which allowed us to obtain a three-orbit disruptive ToO to ensure a good measurement of the SN SED. We also were granted Director's Discretionary time on VLT for imaging in the K_s band (PI: Nordin) with HAWK-I (Kissler-Patig et al. 2008) in order to extend the wavelength range redder than is possible with *HST*. We triggered $F105W$, $F125W$, and $F160W$ imaging from our "See Change" allocation. We did not request *HST* grism spectroscopy, as the roll angle range available would not have allowed for a clean separation of the SN and its host. In addition to our triggered followup, we obtained additional WFC3 $F814W$, $F105W$, and $F140W$ imaging at two more previously scheduled orbits (the cadenced search visits for discovering SNe).

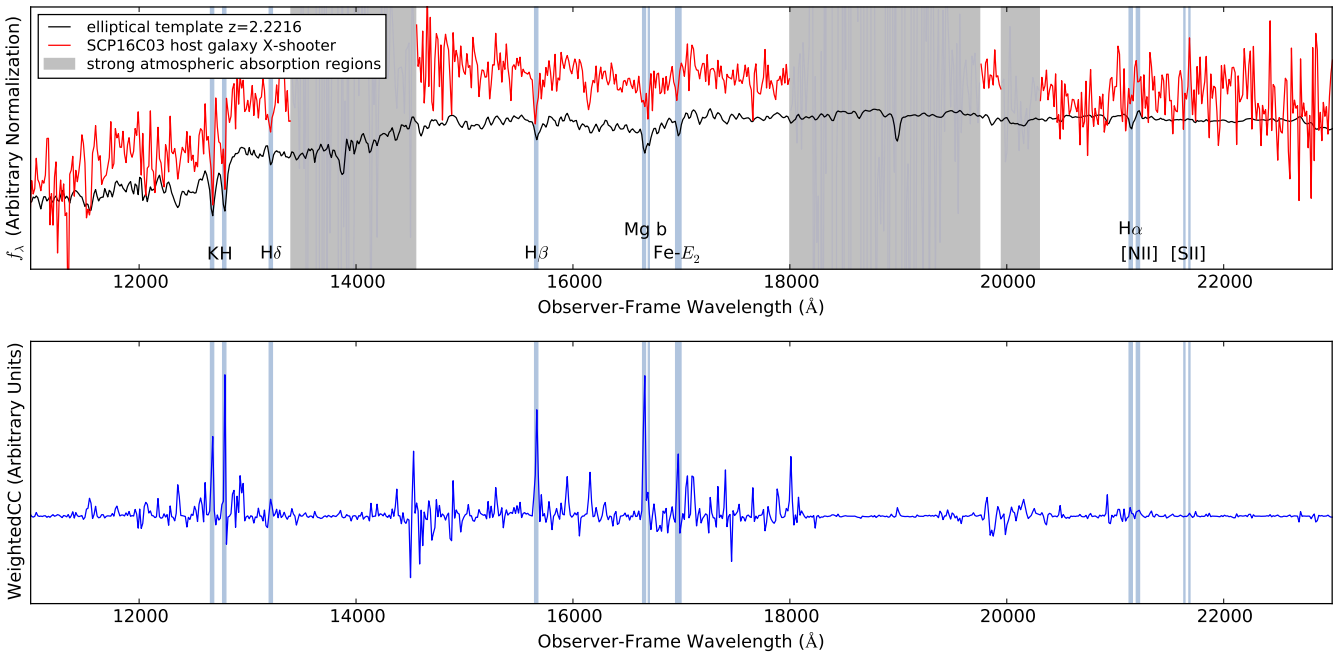

Figure 2. *Top:* Flux-calibrated, telluric corrected, and binned (14Å observer-frame) spectrum of the host galaxy (red line). Gray shaded regions indicate strong atmospheric absorption. The elliptical template used in the weighted cross-correlation is shown in black. Prominent features identified in both spectra are highlighted with light blue shading, and labeled; the Hα complex is labeled for reference, but no prominent contribution to the cross-correlation is detected. *Bottom:* The contribution to the weighted cross correlation of each wavelength element of the spectrum. Regions of heavy atmospheric absorption are properly de-weighted, and the prominent features easily identified by eye provide a confident redshift determination of 2.2216 ± 0.0002. We note that the spectrum does not appear significantly reddened compared to the template, disfavoring a dusty starburst galaxy. This agrees with the broadband SED fit of the host galaxy, which results in a low A_V of 0.05.

4. PHOTOMETRY

With a pixel scale of $\sim 0\farcs128$, the WFC3 IR channel undersamples the PSF, making it difficult to remove underlying galaxy light with image resampling and subtraction. In addition, this SN poses a (unusual, but not unknown) challenge, as we have no reference (SN-free) images in $F125W$ and $F160W$, necessitating interpolation of the galaxy light over the SN position. To meet these needs, we have developed a "forward modeling" code described in Suzuki et al. (2012) and Rubin et al. (2013) and updated for WFC3 IR in Nordin et al. (2014). This code fits each pixel as observed (flat-fielded "flt" images for WFC3 IR, CTE-corrected, flat-fielded "flc" images for WFC3 UVIS), without resampling by creating an analytic model of the scene, convolving that model with the PSF, and fitting it against the pixels. In all cases, the effect on the flatfield of pixel area variations over the FoV are taken into account, as no distortion correction is performed on the input images.

For the host-galaxy, our analytic model is a linear sum of an azimuthally symmetric spline (a 1D, radially varying component that is allowed to have ellipticity) and a 2D grid to capture azimuthal asymmetries.[4] To these splines, we add a point source for the SN, with a different fitted amplitude in each epoch. As there are reference images in the cadenced IR filters ($F105W/F140W$), these can be used as a cross-check of our ability to do reference-free photometry in the filters without references. We obtain virtually the same photometry in the $F105W/F140W$ with and without modeling the reference images, although the uncertainties are smaller when including references. Testing with simulated SNe indicates no photometric biases at the 0.01 magnitude level, and accurate uncertainties,[5] even without using reference images.

There is only weak evidence for SN light in the $F814W$ filter, as expected for a redshift 2.22 SN Ia. The low S/N necessitates a different treatment than the IR, where the offset between the SN and host galaxy is treated as a fit parameter. To determine the location of the SN in $F814W$, we start by aligning the UVIS and IR exposures with `TweakReg`,[6] and drizzling to a common frame with `AstroDrizzle`. (These resampled images are not used for the SN photometry.) Then we perform PSF photometry

[4] The spline nodes were spaced less than 1 pixel ($0\farcs128$) apart for the 1D radially varying spline near the core, and 4 pixels apart for the 2D spline. Reasonable variations around these values returned virtually the same photometry.

[5] We use constant PSFs that do not follow *HST* focus changes. We allow for these changes by adding 0.02 magnitudes (our measured dispersion on bright stars) in quadrature to the fit uncertainties.

[6] All of the software tools referenced here are part of `DrizzlePac`: http://drizzlepac.stsci.edu.

Table 2. Host-galaxy photometry.

Instrument	Filter	Flux (μJy)	Flux Uncertainty (μJy)
OSIRIS	g'	0.19	0.03
OSIRIS	r'	0.37	0.06
OSIRIS	i'	0.55	0.10
WFC3	$F814W$	1.06	0.20
WFC3	$F105W$	3.66	0.08
WFC3	$F140W$	15.05	0.08

NOTE—Measured host-galaxy fluxes in the *HST* and GTC imaging. We scale to μJy (AB zeropoint of 23.9).

on the UVIS images with the centroid transferred from that measured in the IR (using `pixtopix`), where the SN is detected. We fit for a spatially constant background underneath the SN, incorporating both sky and underlying galaxy. Even the core of the galaxy is only detected at low S/N in each $F814W$ exposure, so the second derivative[7] underneath the SN is small.

ESO VLT Director's Discretionary Time was awarded to obtain 7 hrs of HAWK-I K_s photometry. Unfortunately, bad weather allowed only one of seven OBs to be executed and only 40 minutes of effective exposure time was obtained. Nonetheless, the excellent seeing ($0\farcs27$) enables a measurement of SN flux. We use the same host-galaxy model as with the WFC3 IR data, but with the offset of the SN from the host fixed. We use field stars to derive a PSF. We calibrate to the average of field stars in 2MASS (Skrutskie et al. 2006) and the standard star FS19, which give similar zeropoints (we transform this zeropoint to an AB mag zeropoint for convenience). Although the brightness uncertainty is too large to improve the distance measurement, the added rest-frame R coverage helps with photometric classification.

We present the resulting photometry in Table 3. The uncertainty in the host-galaxy subtraction in each band leads to correlations between the WFC3 IR photometry measurements (in the data for each filter), so in addition to uncertainties, we provide the inverse covariance matrix (Table 4). We take the WFC3 IR zeropoints from Nordin et al. (2014), although we convert the zeropoints to AB magnitudes; these take into account the WFC3 IR count-rate nonlinearity. For the F814W filter, we use the the standard UVIS zeropoint, after correcting the encircled energy to an infinite aperture.

We perform our host-galaxy photometry on aligned, stacked (SN-free) images using `SEP`.[8] To minimize contamination by light from the nearby galaxies, we use an elliptical aperture set to 1.2 times the Kron radius (Kron 1980).[9] In addition to the *HST* photometry, we obtained bluer g', r' and i' photometry of the host with the OSIRIS instrument at the Gran Telescopio Canarias (GTC). We determine the zeropoints of this photometry using an SDSS star in the GTC field of view (both the star and galaxy are measured with the same elliptical aperture). We present the photometry in Table 2.

5. HOST GALAXY

5.1. *Spectral Measurements and Star-Formation Rate*

From the X-shooter host-galaxy spectrum, we place an upper limit on the [OII] $\lambda3727$ Å rest-frame equivalent width of EW([OII]) < 5 Å at 95% confidence. After correcting for Balmer stellar absorption (by comparison with the Kinney et al. 1996 elliptical template), we place an upper limit on Hα of EW(Hα) < 8 Å at 95% confidence. The best-fit single-stellar-population Bruzual & Charlot (2003) template has an age of ~ 0.9 Gyr (c.f., the age of the universe at $z = 2.22$ is ~ 3 Gyr). We fit the age just to the region of the 4,000 Å break; it is possible that improving the flux calibration and considering more of the spectrum would improve the measurements enough to give a useful dt/dz measurement for cosmological constraints (Jimenez & Loeb 2002; Stern et al. 2010; Moresco et al. 2012).

[7] As the fit patch is centered on the SN, any slope in the underlying galaxy light will cancel out. Thus, only the second derivative of the light can affect the photometry, and the second derivative at the SN location is much smaller than at the galaxy core.

[8] https://sep.readthedocs.io

[9] The major and minor radii are $1\farcs19$ and $0\farcs83$, respectively.

Table 3. Photometry for SN SCP16C03.

MJD	Flux (ADU/s)	Uncertainty	Chip	AB Zeropoint
		HST $F814W$		
57414.741	0.162	0.079	2	25.146
57446.809	0.079	0.070	1	25.146
57479.413	0.056	0.071	2	25.146
57513.068	0.000	0.066	1	25.146
		VLT K_s		
57479.051	173	102	3	30.26
		HST $F105W$		
57414.751	0.095	0.145	1	26.235
57446.824	0.779	0.197	1	26.235
57465.544	1.543	0.094	1	26.235
57479.426	1.542	0.161	1	26.235
57513.081	0.483	0.156	1	26.235
		HST $F125W$		
57462.864	3.205	0.172	1	26.210
57465.506	3.351	0.173	1	26.210
		HST $F140W$		
57414.756	0.363	0.161	1	26.437
57446.820	3.294	0.245	1	26.437
57479.413	4.835	0.213	1	26.437
57513.068	2.396	0.220	1	26.437
		HST $F160W$		
57462.909	2.673	0.176	1	25.921
57465.572	2.691	0.182	1	25.921

NOTE—Photometry measured for each band on each date. Table 4 has the weight matrices for the WFC3 IR measurements.

Table 4. Inverse covariance matrices for the WFC3 IR photometry.

MJD	Inverse Covariance Matrix				
			$F105W$		
57414.751	48.2472	-1.2956	-5.6335	-1.7874	-1.8504
57446.824	-1.2956	26.0744	-3.3404	-1.0842	-1.1516
57465.544	-5.6335	-3.3404	115.3885	-4.6158	-4.7575
57479.426	-1.7874	-1.0842	-4.6158	39.0092	-1.5386
57513.081	-1.8504	-1.1516	-4.7575	-1.5386	41.7656
			$F125W$		
57462.864	35.4715	-7.4421	···	···	···
57465.506	-7.4421	35.0010	···	···	···
			$F140W$		
57414.756	39.2367	-1.5114	-1.8203	-1.8066	···
57446.820	-1.5114	16.7848	-0.7807	-0.9239	···
57479.413	-1.8203	-0.7807	22.1654	-1.0547	···
57513.068	-1.8066	-0.9239	-1.0547	20.8010	···
			$F160W$		
57462.909	34.5919	-8.5948	···	···	···
57465.572	-8.5948	32.1690	···	···	···

NOTE—Inverse covariance matrices for the WFC3 IR photometric measurements. These data are correlated (within each band) due to uncertainty in the underlying host-galaxy light.

We convert our $H\alpha$ equivalent-width upper limit to an $H\alpha$-luminosity upper limit using the K_s magnitude of the galaxy to flux calibrate the host spectrum, giving $L(H\alpha) < 5.4 \times 10^{40}$ ergs/s.[10] We then convert to an upper limit on the star formation rate using the Calzetti et al. (2010) conversion $\dot{M} = 5.45 \times 10^{-42} L(H\alpha)$ ($M_\odot$/yr)/(erg/s), giving $\dot{M} < 0.3$ $M_\odot$/yr.

5.2. *SED Fit*

We generate galaxy model SEDs using version 3.0 of the code Flexible Stellar Population Synthesis (FSPS[11], Conroy et al. 2009; Conroy & Gunn 2010). We assume the initial mass function (IMF) from Kroupa (2001). We use the BaSeL 3.1 spectral library (Westera et al. 2002) and the MESA Isochrones & Stellar Tracks (MIST, Dotter 2016; Choi et al. 2016). We assume a "delayed-tau" star formation history and allow for a single burst of star formation superimposed. We produce 32,000 composite

[10] The cosmology does not matter much here, but we use a flat ΛCDM cosmology with $\Omega_m = 0.3089$ (Planck Collaboration et al. 2015).

[11] https://github.com/cconroy20/fsps

stellar populations (CSPs) by Monte Carlo sampling from distributions of 6 FSPS parameters: metallicity, dust optical depth, decay rate of star formation, time that star formation begins, time that the burst occurs, and the fraction of mass in the burst.

We fit the *HST* and GTC photometry (after delensing by 1.1 mag, see Section 7) with the redshift fixed, and find a stellar mass of $\log_{10}(M/M_\odot) = 11.3 \pm 0.2$, $\log_{10}(\mathrm{sSFR/yr}^{-1}) = -10.8^{+0.03}_{-0.6}$ (averaged over the last 20 Myr), and age $= 0.9^{+0.6}_{-0.02}$Gyr. The 20 best-fit templates have low extinction, $A_V \sim 0.05$. The best fitting templates are shown in Figure 3.

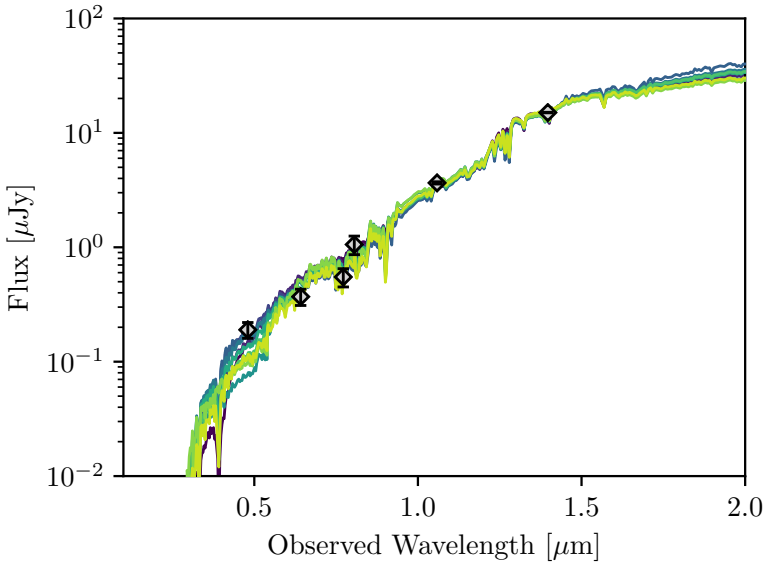

Figure 3. Host-galaxy photometry and the ten best-fitting FSPS SEDs from yellow (best) to dark purple (10th best). The templates are described in Section 5.2. The SED fit implies a low SFR of 0.5 $M_\odot$/yr, consistent with the spectral measurements in Section 5.1, and the surface brightness profile in Section 5.3. These three independent methods all imply a fairly massive, quiescent host galaxy.

5.3. *Profile Fitting*

We also measure the surface brightness profile of the host galaxy. We fit the $F140W$ imaging, as it is close to rest-frame B-band. To determine the central profile given the undersampled imaging, we again use a forward-model approach. We model the observed pixels (without resampling) of nine dithers (from SN-free epochs) with a Sérsic profile (Sérsic 1963) convolved with the PSF (the same PSF as for the SN photometry). We marginalize over the amplitude, effective half-light radius, ellipticity, and orientation[12]. The galaxy is fit well by this simple model, with no evidence of an on-core point source (or variability) which might indicate an AGN (see Figure 4). We find a Sérsic index of 2.8 ± 0.1, more consistent with a bulge-dominated galaxy (~ 4) than a disk-dominated galaxy (~ 1). A Sérsic index such as this is a predictor of a quiescent galaxy, even at $z \sim 2$ (Szomoru et al. 2011; Bell et al. 2012). From Szomoru et al. (2011), an estimate for the $\log_{10}(\mathrm{sSFR/yr}^{-1})$ of a galaxy with a Sérsic index of 2.8 at $z = 2.22$ is ~ -10, consistent with the independent measurements based on both the spectrum and the SED fit.

6. PHOTOMETRIC CLASSIFICATION

It was not possible to obtain a spectrum of the SN itself, so we use our photometry, host-galaxy redshift, and host-galaxy star-formation rate to ascertain the SN type. Making such typing quantitative is made more challenging by the limited signal-to-noise, wavelength coverage, and phase coverage of our light curves. Similarly to the photometric typing efforts performed for other high-redshift SNe (Rodney et al. 2012; Jones et al. 2013; Nordin et al. 2014; Patel et al. 2014; Rodney et al. 2015a), as well as the Photometric Supernova Identifier (Sako et al. 2011), we fit the photometry with a range of templates to compare light curve shape and color. Non-parametric methods have shown comparable promise (e.g., Kessler et al. 2010; Lochner et al. 2016), but better temporal sampling than available here would be necessary to implement these. The core-collapse templates are sourced from SNANA (Kessler et al. 2009), and implemented in SNCosmo[13], some of which are described in Gilliland et al. 1999, Nugent et al.

[12] Marginalizing over the ellipticity also has the effect of making the fit less sensitive to lensing shear.
[13] http://sncosmo.readthedocs.io

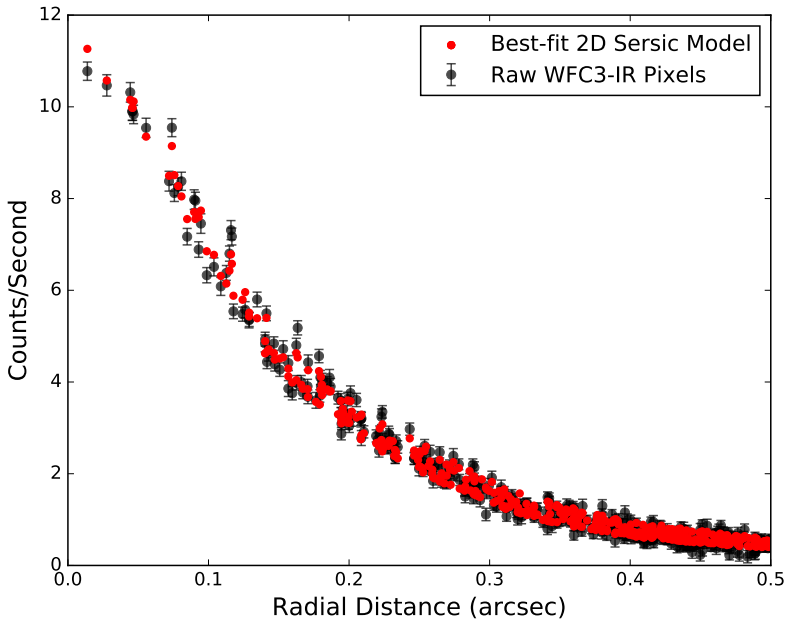

Figure 4. The radial brightness profile of the host galaxy (black points), with the best-fit 2D Sérsic model (red points). The galaxy is well-fit by the 2D Sérsic profile, with a best-fit Sérsic index of 2.8 ± 0.1, consistent with a quiescent galaxy at $z = 2.22$ (Szomoru et al. 2011; Bell et al. 2012), and independent measurements of the sSFR from the X-shooter spectrum (Section 5.1) and broadband SED fit (Section 5.2).

2002, Stern et al. 2004, Levan et al. 2005, and Sako et al. 2011. Typically, the absolute magnitudes of CC SNe are fainter than those of SNe Ia (Richardson et al. 2014), so proportionately fewer are found. Furthermore, the CC SNe that are discovered are less likely to be followed up (because they are not as cosmologically useful), so the CC template set is likely not complete. When multiple versions of the same non-Ia template are available, we conservatively take that with the lowest χ^2. It is also necessary to account for the fact that the parameter space is sampled with only a finite number of templates. As with previous work (Rodney & Tonry 2009), we add 0.15 magnitudes uncertainty in quadrature with each photometry point to address this. We leave the date of maximum and normalization fully unconstrained when fitting the templates against the data. For the relative extinction between SN SCP16C03 and the SN used to determine the template colors, we take a broad, double-sided exponential prior having a scale length of 0.2 in $E(B-V)$. Use of a double-sided exponential allows both the templates and SN SCP16C03 to suffer extinction, and is necessary as the unreddened colors of the templates are unknown. As R_V cannot be constrained by the data, we fix it to the galactic value of 3.1 (for all SN types). For the SN Ia templates, we construct a random sample with the latest version (2-4) of the Spectral Adaptive Lightcurve Template model (Guy et al. 2007; Mosher et al. 2014) (SALT2 is described more in Section 7), with Gaussian distributions of the light-curve shape parameters x_1 and c, centered at zero and having dispersions of 1 in x_1 and 0.1 in c. We also include the Hsiao et al. (2007) SN Ia spectral template, the Nugent et al. (2002) templates for normal SNe Ia and underluminous 1991bg-like SNe Ia, and the Stern et al. (2004) overluminous 1991T-like SN Ia template.[14]

The three best-fitting templates (with a spread in log-likelihood of just 0.2) are the SALT2 SN Ia template (close to the mean of the x_1 and c distributions), the Nugent template for 1991T-like SNe Ia, and an SDSS SN II (SN 2007md). Encouragingly, the best-fit SALT2 template has a χ^2 of 8.7 for 8 DoF (including the SALT2 model uncertainties, but not the 0.15 magnitude uncertainty floor). Other templates with a best-fit likelihood within a factor of 100 of the SN Ia template are the Nugent SN Ia template, an SDSS SN Ib/c template (SN 2006fo), and the Hsiao SN Ia template.[15] It is worth noting that the two CC SNe are $\gtrsim 2$ magnitudes fainter in absolute magnitude than any reasonable value for SN SCP16C03 (we discuss the lensing amplification in Section 8), so our typing analysis may be very conservative since absolute magnitude is not included in the evaluation. However, we do not have enough templates derived from CC SNe in the same absolute magnitude range as SNe Ia, so we include these CC SNe for now.

[14] The Hsiao et al. (2007) and Nugent et al. (2002) normal SN Ia templates are included only as a cross-check, and SALT2 is used for the typing result. SALT2 is parameterized, so we can use it to simulate a distribution of SNe Ia. We do however include the Stern et al. (2004) 1991T-like and Nugent et al. (2002) 1991bg-like templates in the typing result as separate subclasses of SNe Ia that SALT2 does not mimic well.

[15] Interestingly, despite its large uncertainty, the K_s measurement disfavors a single SN Ib/c template (that would be otherwise compatible with the bluer *HST* data for an extinction in excess of 0.5 mag $E(B-V)$); we show the remaining SN Ib/c light-curve template that is not disfavored in Figure 5.

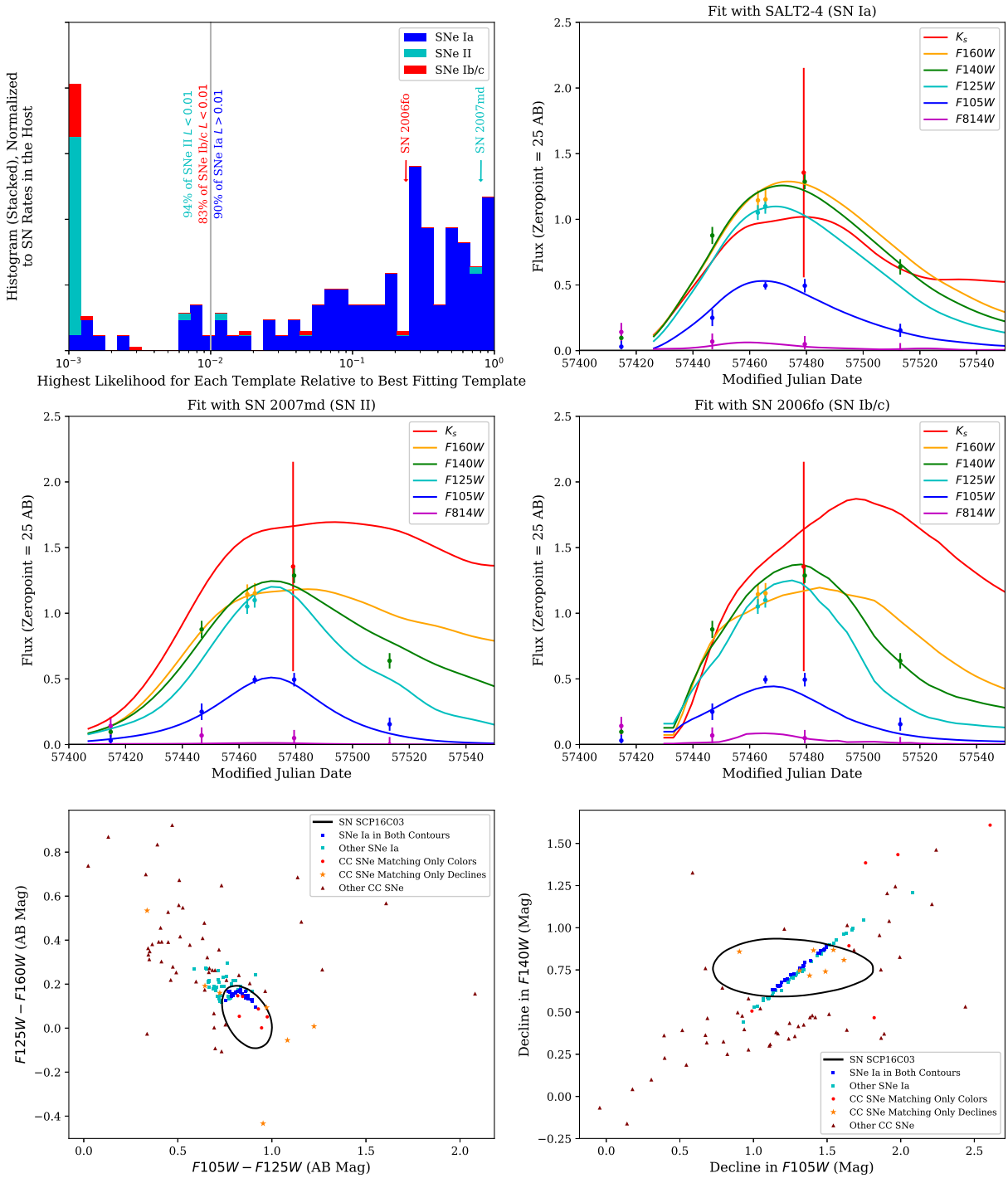

Figure 5. Top left panel: histogram of relative likelihoods for the templates of each type of SN. The likelihoods are scaled so that the template with the highest likelihood has a value of 1. The histogram is normalized such that the area for each type of SN matches the relative rates expected in this galaxy (Section 6). This histogram indicates that, although there are two CC templates with a reasonable fit to the light curves, there are many more that are poor fits and thus the probability that SN SCP16C03 is a SN Ia is high. Light-curve panels: the best-fit for the SN Ia templates (top right), the SN II templates (middle left), and the SN Ib/c templates (middle right). In the bottom panels, we show how SN SCP16C03 compares to the template library in both color (bottom left: the $F105W - F125W$ and $F125W - F160W$ colors at the epoch with all three) and decline rate (bottom right: the decline between the last two epochs in $F105W$ and $F140W$). Each point plotted is from the best-fit (i.e., best-fit amplitude, date of maximum, and extinction) of one of the SN templates (for display purposes, we show as many SNe Ia realizations as CC templates, although most SNe in the host galaxy are SNe Ia). The black contours show the 68% confidence intervals from our measurements of SN SCP16C03. The blue squares represent SNe Ia templates inside both contours; the cyan squares represent SNe Ia outside of at least one contour. The consistency of SN SCP16C03 with the SN Ia distribution is evident. There are no CC SNe in both contours. The red dots represent CC SNe matching the colors, the orange stars represent CC SNe matching the observed declines, and the brown triangles represent CC SNe matching neither colors nor declines.

In order to compute an overall probability of being a SN Ia, we need to estimate the relative rates of CC SNe and SNe Ia in the host galaxy as in Meyers et al. (2012). Starting from the relative rates of SNe Ia[16] and CC SNe,[17] our estimated fraction of SNe Ia is

$$f_{Ia} = \left[1 + \frac{R_{CC}}{R_{Ia}}\right]^{-1} \quad (1)$$

$$= \left[1 + \frac{6.8 \times 10^{-3} \dot{M}}{5.3 \times 10^{-14} M + 3.9 \times 10^{-4} \dot{M}}\right]^{-1} . \quad (2)$$

We take $\log_{10}(M/M_\odot) = 11.3$ and $\dot{M} < 0.3\ M_\odot$/yr from Section 5. With these values, Equation 2 implies that at least 85% of the SNe in the host galaxy will be SNe Ia. We note that this value is essentially independent of the assumed amplification, as both the inferred Hα luminosity and stellar mass have the same scaling with amplification and thus it cancels out of equation 2.

We take a ratio of 3-1 for SNe II to SNe Ib/c (Li et al. 2011). Nearby, 3% of SNe Ia are pure 1991T-like (Scalzo et al. 2012; Silverman et al. 2012), as used to construct the Nugent spectral template. Another 5% of nearby SNe are 1999aa-like (Silverman et al. 2012) while at high redshift we derive a 1999aa-like fraction of 1–3% from Balland et al. (2009). However, 1999aa-like SNe are only marginally overluminous. We therefore assume a 1991T-like fraction of 3% for discoverable (i.e., not 1991bg-like or 2002cx-like) SNe Ia. Thus, our estimated fractions of each type of SN are: 82.5% normal SNe Ia, 2.6% 1991T-like SNe Ia, 11.3% SNe II, and 3.8% SNe Ib/c. Although these fractions are derived at low redshift and may be different at $z = 2.22$, the assumed values do not strongly affect the classification as a SN Ia.

Averaging likelihoods over SN Ib/c, SN II, SN Ia-91T, and SALT2 templates, we find a 91% chance that this is a normal SN Ia, a 7% chance it is a 1991T-like SN Ia, a 0.2% chance of a SN Ib/c, and a 1% chance of a SN II. This analysis is summarized in the top left panel of Figure 5, which shows the highest (best-fit) relative likelihood for each template.

To test whether this SN could be an intra-cluster SN within MOO J1014+0038 having a chance alignment with a background galaxy, we also run the typing at the cluster redshift of 1.23. The best-fit likelihood values are > 100 times lower, strongly disfavoring this possibility.

7. LIGHT-CURVE FIT AND AMPLIFICATION MEASUREMENT

To compute an amplification estimate, and locate SN SCP16C03 in the lower-redshift light-curve parameter distributions, we fit the photometry in Table 3 with the SALT2 light-curve fitter (SALT2-4, the latest version). SALT2 fits a rest-frame model to the observer-frame photometry, extracting a date-of-maximum, amplitude (scaled by the inverse squared luminosity distance and typically quoted using a rest-frame B-band magnitude, m_B), light-curve shape (x_1), and color (c). We find $t_{\rm max} = 57474.6 \pm 1.4$, $m_B = 26.067 \pm 0.041$, $x_1 = 0.54 \pm 0.60$, and $c = 0.039 \pm 0.051$. Our light-curve fit parameters are consistent with the center of the low-redshift x_1 and c distributions, disfavoring strong evolution in the population mean of these parameters.[18] This test would have been difficult to perform with unlensed SNe in this redshift range due to selection effects (the 50% completeness limit at this redshift for unlensed SNe is about -19.1, similar to the median absolute magnitude of SNe Ia; Rodney et al. 2015b, Hayden et al. in prep.) and the difficulty of photometrically typing SNe ~ 1 magnitude fainter than the amplified SN SCP16C03.

In many previous analyses, linear shape and color standardization has been employed (Tripp 1998), i.e.,

$$\mu_B = m_B + \alpha\, x_1 - \beta\, c - M_B \quad (3)$$

where α and β are the slope of the shape and color standardization relations, and M_B is the absolute B-band magnitude. Here we assume $H_0 = 70$ km s^{-1} Mpc^{-1}, but it drops out of the final analysis of the amplification. We take our values of the standardization coefficients from Betoule et al. (2014). Evidence is steadily increasing that the x_1 and c relations are not linear; at a minimum, broken-linear relations are more accurate (Amanullah et al. 2010; Suzuki et al. 2012; Scolnic et al. 2014; Rubin et al. 2015; Scolnic & Kessler 2016; Mandel et al. 2016). For simplicity, we use linear relations here, as this SN is close to the center of both the x_1 and c distributions, so applying non-linear relations makes little difference. The observed absolute

[16] Here, we use the "prompt-and-delayed" model, in which the SN Ia rate is modeled as a linear combination of solar mass and star-formation rate (Scannapieco & Bildsten 2005; Mannucci et al. 2006). We use coefficients from the Sullivan et al. (2006) analysis. This is a simple approximation to the true delay-time distribution, which is close to t^{-1} (see the review of Maoz & Mannucci 2012). We also try using our age and stellar mass with a t^{-1} delay-time distribution (normalized as in Rodney et al. 2014), and find a somewhat higher SN Ia rate. We use the prompt-and-delayed rate to be conservative.

[17] Assuming a Salpeter IMF (Salpeter 1955) with all stars from 8 $M_\odot$ to 40 $M_\odot$ forming CC SNe, there will be 6.8×10^{-3} CC SNe per $M_\odot$ of formed stars. This assumption is a reasonable match to observed CC rates and the cosmic star-formation history (Madau & Dickinson 2014; Strolger et al. 2015).

[18] In order to quantify this, we have to deconvolve by the measurement uncertainties. When we do this assuming a split-normal distribution (https://github.com/rubind/salt2params), we find that SN SCP16C03 is at the 64 ± 20th percentile in x_1, and the 67^{+16}_{-22}th percentile in c. If the (mild) evidence for SN light in the epoch before the detection is real, the rise-time is ~ 20 days in rest-frame B-band. This is slower than average for a SN Ia, but still within the observed distribution (Hayden et al. 2010).

magnitude has a weak dependence on host-galaxy stellar mass (Kelly et al. 2010; Sullivan et al. 2010), but this relation may be partially driven by progenitor age, and thus would weaken with redshift as young progenitors will dominate galaxies of both high and low stellar mass (Rigault et al. 2013; Childress et al. 2014). However, the lack of detectable emission lines in the host of SN SCP16C03 decreases the likelihood that it arose from a young progenitor system. Although most of the likelihood for our galaxy is in the high-mass category ($> 10^{10} M_{\odot}$), we split the difference in M_B, taking the average of the two host-mass categories (for a value of -19.085), and allocating half of the difference as uncertainty (0.035 magnitudes). We assume 0.12 magnitudes of "intrinsic" dispersion in the absolute magnitude of high-redshift SNe Ia (Rubin et al. in prep.). We also consider the various WFC3 IR systematic uncertainties highlighted in Nordin et al. (2014): count-rate nonlinearity, flux-dependent PSF, SED-dependent PSF, and the uncertainty in the Calspec system (Bohlin 2007; Bohlin et al. 2014). We evaluate the impact of each systematic uncertainty on the distance modulus by varying each one and refitting the SN distance. We then include these differences in the quadrature sum for the total distance uncertainty.

In order to complete the amplification measurement, we need an estimate of the distance modulus (in the absence of lensing). One method for obtaining this is to compare against a sample of unlensed SNe at similar redshifts (Patel et al. 2014; Rodney et al. 2015a), but no such sample exists for SN SCP16C03. We thus compute the estimated amplification by comparing the SN distance modulus estimate with a cosmological model. We take $\Omega_m = 0.3089$ from Planck Collaboration et al. (2015) (including all cosmological datasets), and for simplicity we assume a flat ΛCDM cosmology, but we use a large ± 0.03 Gaussian uncertainty on Ω_m. This yields a predicted distance modulus of $\mu = 46.219 \pm 0.057$, again for $H_0 = 70$ km s^{-1} Mpc^{-1} (as noted above, H_0 drops out of the analysis). As the uncertainty on our measured distance modulus is much larger than the uncertainty on this prediction, the impact of our assumptions is minor. We obtain a distance modulus estimate of 45.11 ± 0.22 mag, and an amplification estimate of 1.10 ± 0.23 mag, with almost all of the measurement uncertainty (0.22 mag) statistical, and not from the cosmological model or systematic uncertainties.

8. AMPLIFICATION INTERPRETATION

As noted in Nordin et al. (2014), we can either test a lensing-derived model with the measured supernova amplification, or improve the lensing-derived model by including our amplification measurement. For the moment, we choose the former, comparing against the weak-lensing (WL) measurements of Kim et al. (in prep.), which are derived independently from this analysis. That analysis is based on galaxy shear measurements from the $F105W$ and $F140W$ imaging data; the total exposure time of each filter exceeded 16,000 s at the time of the analysis. The PSFs are modeled separately using globular cluster observations originally planned for the WFC3 on-orbit calibration. We measure a galaxy shear by fitting a PSF-convolved elliptical Gaussian profile to a galaxy image. After verifying the consistency of the results from both filters, we optimally combine the two shear measurements and create a single source catalog. The redshift distribution of the source population is estimated by utilizing the publicly available UVUDF photometric redshift catalog (Rafelski et al. 2015). Because of the limited angular scale, we assume a mass-concentration relation of Duffy et al. (2008) in our mass estimation of the cluster while fitting an NFW profile to tangential shears.

Given that the contours of the WL shear map appear to be reasonably smooth, we assume spherical symmetry for the cluster. We use Monte-Carlo methods to derive the predicted amplification at the location of the SN image, assuming Gaussian constraints on the centroid of the cluster and the virial mass, and find $0.61^{+0.20}_{-0.16}$ mag. This value is compatible at $1.6\,\sigma$ with the SN amplification measurement (assuming that the uncertainty on the difference is the quadrature sum of the amplification uncertainties). We note that a concentration of bright cluster galaxies lies slightly to the west of the lens center determined from weak lensing analysis. Their proximity to the SN may boost its amplification. We show contours of the full map (from the median of the Monte-Carlo samples) in Figure 1. We have also used the amplification determined from the SN observations to try to estimate the concentration parameter, c_{200}. While at the current level of observation it is not possible to place strong constraints on the concentration, the inferred value for c_{200} is consistent with N-body simulations based on ΛCDM at $z = 1.23$.

In previous work with high-redshift SNe, (e.g., Suzuki et al. 2012; Rubin et al. 2013; Nordin et al. 2014), we were able to make use of "blinded" analyses, in which the results are hidden until the analysis is finalized (e.g., Conley et al. 2006; Maccoun & Perlmutter 2015). In those works, we were able to blind both the final photometry and the final typing, as both improved over the course of the analysis. In our analysis of SN SCP16C03, we approached the photometry and typing with a mature pipeline, and made the decision to trigger followup based on this pipeline. Those results cannot be taken to be blinded, although we know of no biases that were introduced. By contrast, the lensing comparison was only conducted after the rest of the analysis was frozen and is thus fully blinded.

9. SUMMARY

We present our discovery and measurements of a lensed SN with a host-galaxy redshift of 2.22. The light curve of this SN most closely matches a SN Ia, in both shape and color; there are only two known core collapse templates within a factor of 100 of the best fit SN Ia likelihood (and with both of these requiring an additional two magnitudes of amplification to match the absolute magnitude of SNe Ia). We determine a robust host galaxy redshift of 2.2216 ± 0.0002, from a VLT X-shooter spectrum displaying multiple absorption features. Measurements of the spectrum, SED fitting of the broadband photometry (from GTC OSIRIS g', r' and i' and *HST* $F105W$ and $F140W$), and measurement of the surface brightness profile independently demonstrate a massive, low-SFR host galaxy. When combined with observational constraints on SN rates, the low-SFR environment implies that most of the SNe in this galaxy are expected to be SNe Ia. When considering the likelihoods from the light curve fits to all SN subtypes, this leads to a 99% probability that this exceptional event is a SN Ia. This makes it the highest redshift SN Ia with a spectroscopic redshift and the highest redshift lensed SN of any type. Using the conventional SN Ia standardization relation and assuming a Planck Collaboration et al. (2015) cosmology, we estimate the SN amplification is $2.8^{+0.6}_{-0.5}$ in flux (1.1 mag), making this the most amplified SN Ia discovered behind a galaxy cluster to date. We estimate only a 10% chance of finding a SN Ia at or beyond this redshift (using the high-redshift SN rate model in Rodney et al. (2014) up to $z = 3$) at least this close to the center of one of our clusters (thus allowing it to be lensed), making this an exceptional discovery. The light-curve parameters of SN SCP16C03 are close to the mode of the population distribution of lower redshift SNe, indicating that our first unbiased look at the $z \sim 2$ SN Ia population shows no evidence of strong population drift in these parameters. We also find consistency between the estimated amplification from the weak-lensing-derived map and our Hubble diagram residual. Based on our work, it appears that there were normal SNe Ia ~ 11 Gyr before the present.

Based on observations made with the NASA/ESA *Hubble Space Telescope*, obtained at the Space Telescope Science Institute, which is operated by the Association of Universities for Research in Astronomy, Inc., under NASA contract NAS 5-26555. These observations are associated with programs GO-13677 and GO-14327. Additionally based on observations collected at the European Organisation for Astronomical Research in the Southern Hemisphere under ESO program IDs 096.A-0926 and 296.A-5051. This publication makes use of data products from the Two Micron All Sky Survey, which is a joint project of the University of Massachusetts and the Infrared Processing and Analysis Center/California Institute of Technology, funded by the National Aeronautics and Space Administration and the National Science Foundation. Based on observations made with the Gran Telescopio Canarias (GTC), installed at the Spanish Observatorio del Roque de los Muchachos of the Instituto de Astrofsica de Canarias, on the island of La Palma. Additional support was provided from NASA ADAP NNH16AC25I. Support for programs GO-13677, GO-14327, and SNAP-14163 were provided by NASA through a grant from the Space Telescope Science Institute, which is operated by the Association of Universities for Research in Astronomy, Inc., under NASA contract NAS 5-26555. Additional support was provided by the Director, Office of Science, Office of High Energy Physics, of the U.S. Department of Energy under contract No. DE-AC02-05CH11231. M. J. Jee acknowledges support from KASI and NRF of Korea to CGER. The work of P.E. and D.S. was carried out at Jet Propulsion Laboratory, California Institute of Technology, under a contract with NASA. We also acknowledge the anonymous referee, whose feedback greatly improved this manuscript.

Facilities: HST (WFC3), VLT:Kueyen, VLT:Yepun, GTC

REFERENCES

Amanullah, R., Lidman, C., Rubin, D., et al. 2010, ApJ, 716, 712
Amanullah, R., Goobar, A., Clément, B., et al. 2011, ApJL, 742, L7
Balland, C., Baumont, S., Basa, S., et al. 2009, A&A, 507, 85
Bell, E. F., van der Wel, A., Papovich, C., et al. 2012, ApJ, 753, 167
Betoule, M., Kessler, R., Guy, J., et al. 2014, A&A, 568, A22
Bohlin, R. C. 2007, in Astronomical Society of the Pacific Conference Series, Vol. 364, The Future of Photometric, Spectrophotometric and Polarimetric Standardization, ed. C. Sterken, 315
Bohlin, R. C., Gordon, K. D., & Tremblay, P.-E. 2014, PASP, 126, 711
Brodwin, M., Greer, C. H., Leitch, E. M., et al. 2015, ApJ, 806, 26
Bruzual, G., & Charlot, S. 2003, MNRAS, 344, 1000
Calzetti, D., Wu, S.-Y., Hong, S., et al. 2010, ApJ, 714, 1256
Childress, M. J., Wolf, C., & Zahid, H. J. 2014, MNRAS, 445, 1898
Choi, J., Dotter, A., Conroy, C., et al. 2016, ApJ, 823, 102
Clough, S. A., Iacono, M. J., & Moncet, J.-L. 1992, Journal of Geophysical Research: Atmospheres, 97, 15761
Clough, S. A., Shephard, M. W., Mlawer, E. J., et al. 2005, JQSRT, 91, 233
Conley, A., Goldhaber, G., Wang, L., et al. 2006, ApJ, 644, 1
Conroy, C., & Gunn, J. E. 2010, ApJ, 712, 833
Conroy, C., Gunn, J. E., & White, M. 2009, ApJ, 699, 486
Decker, B., et al. in prep.

Dotter, A. 2016, ApJS, 222, 8
Duffy, A. R., Schaye, J., Kay, S. T., & Dalla Vecchia, C. 2008, MNRAS, 390, L64
Freudling, W., Romaniello, M., Bramich, D. M., et al. 2013, A&A, 559, A96
Gettings, D. P., Gonzalez, A. H., Stanford, S. A., et al. 2012, ApJL, 759, L23
Gilliland, R. L., Nugent, P. E., & Phillips, M. M. 1999, ApJ, 521, 30
Gonzalez, A. H., Decker, B., Brodwin, M., et al. 2015, ApJL, 812, L40
Goobar, A., Paech, K., Stanishev, V., et al. 2009, A&A, 507, 71
Goobar, A., Amanullah, R., Kulkarni, S. R., et al. 2017, Science, 356, 291
Gullikson, K., Dodson-Robinson, S., & Kraus, A. 2014, AJ, 148, 53
Guy, J., Astier, P., Baumont, S., et al. 2007, A&A, 466, 11
Hayden, B., et al. in prep.
Hayden, B. T., Garnavich, P. M., Kessler, R., et al. 2010, ApJ, 712, 350
Hsiao, E. Y., Conley, A., Howell, D. A., et al. 2007, ApJ, 663, 1187
Jimenez, R., & Loeb, A. 2002, ApJ, 573, 37
Jones, D. O., Rodney, S. A., Riess, A. G., et al. 2013, ApJ, 768, 166
Kelly, P. L., Hicken, M., Burke, D. L., Mandel, K. S., & Kirshner, R. P. 2010, ApJ, 715, 743
Kelly, P. L., Rodney, S. A., Treu, T., et al. 2015, Science, 347, 1123
—. 2016a, ApJL, 819, L8
Kelly, P. L., Brammer, G., Selsing, J., et al. 2016b, ApJ, 831, 205
Kessler, R., Bernstein, J. P., Cinabro, D., et al. 2009, PASP, 121, 1028
Kessler, R., Bassett, B., Belov, P., et al. 2010, PASP, 122, 1415
Kim, S., et al. in prep.
Kinney, A. L., Calzetti, D., Bohlin, R. C., et al. 1996, ApJ, 467, 38
Kissler-Patig, M., Pirard, J.-F., Casali, M., et al. 2008, A&A, 491, 941
Kron, R. G. 1980, ApJS, 43, 305
Kroupa, P. 2001, MNRAS, 322, 231
Levan, A., Nugent, P., Fruchter, A., et al. 2005, ApJ, 624, 880
Li, W., Leaman, J., Chornock, R., et al. 2011, MNRAS, 412, 1441
Lochner, M., McEwen, J. D., Peiris, H. V., Lahav, O., & Winter, M. K. 2016, ArXiv e-prints, arXiv:1603.00882
Maccoun, R., & Perlmutter, S. 2015, Nature, 526, 187
Madau, P., & Dickinson, M. 2014, ARA&A, 52, 415
Mandel, K. S., Scolnic, D., Shariff, H., Foley, R. J., & Kirshner, R. P. 2016, ArXiv e-prints, arXiv:1609.04470
Mannucci, F., Della Valle, M., & Panagia, N. 2006, MNRAS, 370, 773
Maoz, D., & Mannucci, F. 2012, PASA, 29, 447
Meyers, J., Aldering, G., Barbary, K., et al. 2012, ApJ, 750, 1
Moresco, M., Cimatti, A., Jimenez, R., et al. 2012, JCAP, 8, 006
Mosher, J., Guy, J., Kessler, R., et al. 2014, ApJ, 793, 16
Navarro, J. F., Frenk, C. S., & White, S. D. M. 1997, ApJ, 490, 493
Nordin, J., Rubin, D., Richard, J., et al. 2014, MNRAS, 440, 2742
Nugent, P., Kim, A., & Perlmutter, S. 2002, PASP, 114, 803
Patel, B., McCully, C., Jha, S. W., et al. 2014, ApJ, 786, 9
Petrushevska, T., Amanullah, R., Goobar, A., et al. 2016, A&A, 594, A54
Planck Collaboration, Ade, P. A. R., Aghanim, N., et al. 2015, ArXiv e-prints, arXiv:1502.01589
Quimby, R. M., Oguri, M., More, A., et al. 2014, Science, 344, 396
Rafelski, M., Teplitz, H. I., Gardner, J. P., et al. 2015, AJ, 150, 31
Richardson, D., Jenkins, III, R. L., Wright, J., & Maddox, L. 2014, AJ, 147, 118
Rigault, M., Copin, Y., Aldering, G., et al. 2013, A&A, 560, A66
Rodney, S. A., & Tonry, J. L. 2009, ApJ, 707, 1064
Rodney, S. A., Riess, A. G., Dahlen, T., et al. 2012, ApJ, 746, 5
Rodney, S. A., Riess, A. G., Strolger, L.-G., et al. 2014, AJ, 148, 13
Rodney, S. A., Patel, B., Scolnic, D., et al. 2015a, ApJ, 811, 70
Rodney, S. A., Riess, A. G., Scolnic, D. M., et al. 2015b, AJ, 150, 156
Rubin, D., Knop, R. A., Rykoff, E., et al. 2013, ApJ, 763, 35
Rubin, D., Aldering, G., Barbary, K., et al. 2015, ApJ, 813, 137
Rubin, D., et al. in prep.
Sako, M., Bassett, B., Connolly, B., et al. 2011, ApJ, 738, 162
Salpeter, E. E. 1955, ApJ, 121, 161
Scalzo, R., Aldering, G., Antilogus, P., et al. 2012, ApJ, 757, 12
Scannapieco, E., & Bildsten, L. 2005, ApJL, 629, L85
Scolnic, D., & Kessler, R. 2016, ApJL, 822, L35
Scolnic, D. M., Riess, A. G., Foley, R. J., et al. 2014, ApJ, 780, 37
Sérsic, J. L. 1963, Boletin de la Asociacion Argentina de Astronomia La Plata Argentina, 6, 41
Silverman, J. M., Kong, J. J., & Filippenko, A. V. 2012, MNRAS, 425, 1819
Skrutskie, M. F., Cutri, R. M., Stiening, R., et al. 2006, AJ, 131, 1163
Stanford, S. A., Gonzalez, A. H., Brodwin, M., et al. 2014, ApJS, 213, 25
Stanishev, V., Goobar, A., Paech, K., et al. 2009, A&A, 507, 61
Stern, D., Jimenez, R., Verde, L., Kamionkowski, M., & Stanford, S. A. 2010, JCAP, 2, 008
Stern, D., van Dokkum, P. G., Nugent, P., et al. 2004, ApJ, 612, 690
Strolger, L.-G., Dahlen, T., Rodney, S. A., et al. 2015, ApJ, 813, 93
Sullivan, M., Le Borgne, D., Pritchet, C. J., et al. 2006, ApJ, 648, 868
Sullivan, M., Conley, A., Howell, D. A., et al. 2010, MNRAS, 406, 782
Suzuki, N., Rubin, D., Lidman, C., et al. 2012, ApJ, 746, 85
Szomoru, D., Franx, M., Bouwens, R. J., et al. 2011, ApJL, 735, L22
Tripp, R. 1998, A&A, 331, 815

Vernet, J., Dekker, H., D'Odorico, S., et al. 2011, A&A, 536, A105
Westera, P., Lejeune, T., Buser, R., Cuisinier, F., & Bruzual, G. 2002, A&A, 381, 524
Wright, E. L., Eisenhardt, P. R. M., Mainzer, A. K., et al. 2010, AJ, 140, 1868